Fading Correlation and Its Effect on the Capacity of Multielement Antenna Systems

Da-Shan Shiu, *Member, IEEE*, Gerard J. Foschini, *Fellow, IEEE*, Michael J. Gans, and
Joseph M. Kahn, *Senior Member, IEEE*

Abstract—We investigate the effects of fading correlations in multielement antenna (MEA) communication systems. Pioneering studies showed that if the fades connecting pairs of transmit and receive antenna elements are independently, identically distributed, MEA's offer a large increase in capacity compared to single-antenna systems. An MEA system can be described in terms of spatial eigenmodes, which are single-input single-output subchannels. The channel capacity of an MEA is the sum of capacities of these subchannels. We will show that the fading correlation affects the MEA capacity by modifying the distributions of the gains of these subchannels. The fading correlation depends on the physical parameters of MEA and the scatterer characteristics. In this paper, to characterize the fading correlation, we employ an abstract model, which is appropriate for modeling narrow-band Rayleigh fading in fixed wireless systems.

I. INTRODUCTION

RECENTLY, multielement antenna (MEA) systems that use diversity at both the transmitter and the receiver have drawn considerable attention. Consider an MEA that has n_T and n_R antenna elements at the transmitter and the receiver, respectively. It has been shown that, as $n = \min(n_T, n_R)$ grows toward infinity, for a given fixed average transmitter power, if the fades between pairs of transmit–receive antenna elements are independent and identically Rayleigh, the average channel capacity divided by n approaches a nonzero constant determined by the average signal-to-noise ratio (SNR) [1], [2]. This large capacity growth occurs even if the transmitter has no knowledge of the channel.

The aforementioned assumption of independent and identically distributed i.i.d. fading has been made in many previous works that explore the capacity of MEA (e.g., [1], [3], [4]). However, in real propagation environments, the fades are not independent due, for example, to insufficient spacing between antenna elements. It has been observed [5] that when the fades are correlated, the channel capacity can be significantly smaller than when the fades are i.i.d. The goal of this paper is to analytically investigate the effects of fading correlations on MEA. To do this, we first need to determine the fading correlation.

There have been many works that study the characteristics of spatial fading correlation, mainly motivated by the need to quantify the effect of fading correlation on the performance of diversity reception systems ($n_T = 1$, $n_R > 1$). One approach is to record a large number of typical channel realizations through field measurements or through ray-tracing simulations, e.g., [5]–[9]. Another approach is to construct a scatterer model that can provide a reasonable description of the scattering environments for the wireless application of interest. The advantage of using abstract models is that with a simple and intuitive model, the essential characteristics of the channel can be clearly illuminated, and the insights obtained from the model can then be utilized in planning the detailed measurements and/or simulations. For an overview of the numerous scattering models, see [10]. Examples of the abstract model approach include [6] and [11]–[14]. It must be noted, however, that abstract models need to be validated. To our knowledge, the modeling of fading correlation and its effect on capacity when both the transmitter and receiver employ multiple antenna elements have not been addressed by previous works.[1]

In this paper, to model multipath propagation and fading correlation, we extend the "one-ring" model first employed by Jakes [11]. This model is appropriate in the fixed wireless communication context, where the base station is elevated and seldom obstructed. The spatial fading correlation of a narrow-band flat fading channel can be determined from the physical parameters of the model, which includes antenna spacing, antenna arrangement, angle spread, and angle of arrival. In this paper, we will derive the capacity distribution given the spatial fading correlation; the spatial fading correlation can also be applied in research areas related to other MEA applications [16].

In order to quantify the effect of fading correlation, we focus on the information-theoretic channel capacity. In this paper, the channel capacity is treated as a random quantity, which is a function of the random channel realization. We will show that an n_T-input n_R-output multiple antenna system consists of $n = \min(n_T, n_R)$ subchannels, or eigenmodes. The channel capacity of the MEA is the sum of the individual subchannel capacities. Fading correlation determines the distributions of the subchannel capacities and thus the distribution of the

[1]Driessen and Foschini [15] studied the deterministic channel when only line-of-sight channel components exist between the transmitting antenna elements or their images and the receiving antenna elements.

MEA capacity. We formulate the upper and lower bounds of the MEA capacity and present the distributions of the bounds. However, the distributions of the exact values of MEA capacity and subchannel capacities are very difficult to compute, and we employ Monte Carlo simulations to observe histograms of these quantities.

The remainder of this paper is organized as follows. In Section II, we define the notation for MEA systems and introduce the necessary mathematical background. We present the abstract multipath propagation model from which the spatial fading correlation is derived. In Section III, we present the analysis of MEA capacity, most importantly the closed-form expressions for the distributions of the bounds on MEA capacity given the spatial fading correlation. In Section IV we employ Monte Carlo simulations to obtain the histograms of MEA capacity. Concluding remarks can be found in Section V.

II. DEFINITIONS, ASSUMPTIONS, AND BACKGROUND

A. System Model

An MEA system that employs n_T transmitting and n_R receiving antenna elements is referred to as an (n_T, n_R) MEA. In this paper, we focus on single-user to single-user communication, i.e., the n_T transmitting antennas are collocated, as are the n_R receiving antennas. In this paper, we assume that the communication is carried out using bursts (packets) and that the channel varies at a rate slow enough that it can be regarded as essentially fixed during a burst. Under this assumption, an MEA system is linear time-invariant during a burst transmission. Let the signal transmitted by the lth transmitting antenna element TA_l be denoted by $s^l(t)$, and the signal received by the mth receiving antenna element RA_m be denoted by $r^m(t)$. The impulse response connecting the input of the channel from TA_l to the output of the channel to RA_m is denoted by $h^{m,l}(t)$. The input/output relation of the MEA system is described by the following vector notation:

$$\boldsymbol{r}(t) = H(t) * \boldsymbol{s}(t) + \boldsymbol{v}(t) \qquad (1)$$

where $*$ denotes convolution, $\boldsymbol{r}(t) = (r^1(t)r^2(t)\cdots r^{n_R}(t))'$, $\boldsymbol{s}(t) = (s^1(t)s^2(t)\cdots s^{n_T}(t))'$, $H_{m,l}(t) = h^{m,l}(t)$, and $\boldsymbol{v}(t)$ is additive white Gaussian noise (AWGN). We use x^* to denote the conjugate of a number x, and $\boldsymbol{x}'$ and $x^\dagger$ to denote the transpose and conjugate transpose of a vector $\boldsymbol{x}$, respectively. If the communication bandwidth is narrow enough that the channel frequency response can be treated as flat across frequency, the discrete-time system corresponding to (1) is

$$\boldsymbol{r}_\tau = H\boldsymbol{s}_\tau + \boldsymbol{v}_\tau \qquad (2)$$

where τ is the discrete-time index.

A real Gaussian random variable with mean ζ and variance σ^2 is denoted as $N(\zeta, \sigma^2)$. A circularly symmetric complex Gaussian random variable z, denoted by $z \sim \tilde{N}(0, \sigma^2)$, is a random variable $z = x + iy$ in which x and y are i.i.d. $N(0, \sigma^2/2)$. When the fading is Rayleigh, the channel gain $H_{m,l}$ is modeled as $\tilde{N}(0, 1)$ [17]. The n_R noise components of $\boldsymbol{v}_t$ are assumed to be i.i.d. $\tilde{N}(0, 1)$. The average transmitted
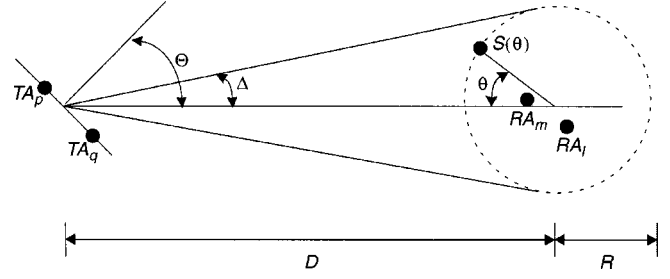

Fig. 1. Illustration of the abstract "one-ring" model. The size of the antenna sets are exaggerated for clarity. TA_p: transmitting antenna p. RA_l: receiving antenna l. $S(\theta)$: the scatterer at angle θ. δ: angle spread. $D_{X \to Y}$: the distance from object X to object Y.

power, which is equal to the average SNR with this normalization of noise power and channel loss, is limited to be no greater than ρ, regardless of n_T.

B. Abstract Scatterer Model

Fig. 1 shows the "one-ring" model. This model will be employed to determine the spatial fading correlation of the channel H. As we mentioned in the introduction, this model has been employed in several studies with some minor variations. The "one-ring" model is appropriate in the fixed wireless communication context, where the base station (BS) is usually elevated and unobstructed by local scatterers, and the subscriber unit (SU) is often surrounded by local scatterers. For notational convenience, in this paper, the BS and the SU assume the roles of transmitter and receiver, respectively. This designation of roles does not affect the capacity because the expression for the MEA capacity is invariant under transposition of H, as will be shown in Section III. The parameters in the model include the distance D between BS and SU, the radius R of the scatterer ring, the angle of arrival Θ at the BS, and the geometrical arrangement of the antenna sets. As seen by a particular antenna element, the angles of incoming waves are confined within $[\Theta - \Delta, \Theta + \Delta]$. We refer to Δ as the angle spread. Since D and R are typically large compared to the antenna spacing, $\Delta \approx \arcsin(R/D)$. The "one-ring" model is basically a ray-tracing model. The following assumptions are generally made in this model [6], [12].

- Every actual scatterer that lies at an angle θ to the receiver is represented by a corresponding effective scatterer located at the same angle on the scatterer ring centered on the SU. Actual scatterers, and thus effective scatterers, are assumed to be distributed uniformly in θ. The effective scatterer located at angle θ is denoted by $S(\theta)$. A phase $\phi(\theta)$ is associated with $S(\theta)$; $\phi(\theta)$ represents the dielectric properties and the radial displacement from the scatterer ring of the actual scatterer that $S(\theta)$ represents [6]. Therefore, rays that are reflected by $S(\theta)$ are all subject to a phase change of $\phi(\theta)$. Statistically, $\phi(\theta)$ is modeled as uniformly distributed in $[-\pi, \pi)$ and i.i.d. in θ. The radius R of the scatterer ring is determined by the root-mean-square (rms) delay spread of the channel [6].
- Only rays that are reflected by the effective scatterers exactly once are considered.
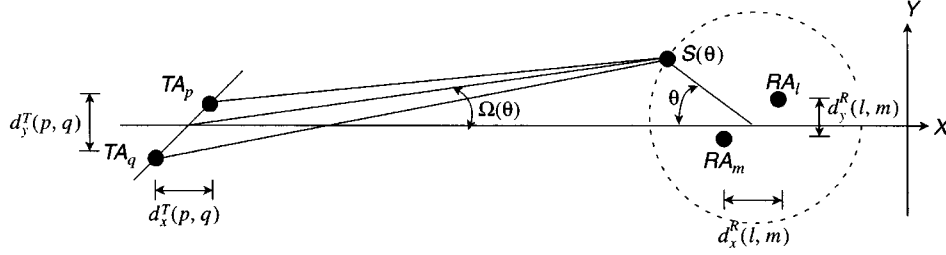- All rays that reach the receiving antennas are equal in power.

Fig. 2. Parameters used to derive the approximations for $E[H_{l,p}H^*_{m,q}]$ in the "one-ring" model.

Suppose that there are K effective scatterers $S(\theta_k)$, $k = 1, 2, \cdots, K$. The properly normalized complex path gain $H_{l,p}$ connecting transmitting antenna element TA_p and receiving antenna element RA_l is

$$H_{l,p} = \frac{1}{\sqrt{2\pi}} \int_0^{2\pi} \frac{1}{\sqrt{K}} \sum_{k=1}^{K} \delta(\theta - \theta_k) \exp\left\{-j\frac{2\pi}{\lambda}\right.$$
$$\left. \cdot \left(D_{\mathrm{TA}_p \to S(\theta)} + D_{S(\theta) \to \mathrm{RA}_l}\right) + j\phi(\theta)\right\} d\theta. \quad (3)$$

In (3), $D_{X \to Y}$ is the distance from object X to object Y, and λ is the wavelength. By the central limit theorem, in the limit of infinitely many scatterers, $H_{l,p}$ constructed from (3) is $\tilde{N}(0, 1)$. Therefore, in the limit case, the channel constructed according to the model is purely Rayleigh fading [17], [18]. To study the fading correlation, we use the following notation. If H is an $n_R \times n_T$ matrix, then we use $\mathrm{vec}(H)$ to denote $n_R n_T \times 1$ the vector formed by stacking the columns of H under each other; that is, if $H = (\boldsymbol{h}_1, \boldsymbol{h}_2, \cdots, \boldsymbol{h}_{n_T})$, where $\boldsymbol{h}_i$ is an $n_R \times 1$ vector for $i = 1, \cdots, n_T$, then

$$\mathrm{vec}(H) = \left(\boldsymbol{h}_1', \boldsymbol{h}_2', \cdots, \boldsymbol{h}_{n_T}'\right)'. \quad (4)$$

The covariance matrix of H is defined as the covariance matrix of the vector $\mathrm{vec}(H)$: $\mathrm{cov}(\mathrm{vec}(H)) = \boldsymbol{E}[\mathrm{vec}(H)\mathrm{vec}(H)^\dagger]$. (Note that for a zero-mean complex Gaussian vector $\boldsymbol{g}$, the autocovariance is specified as the autocovariance matrix of the vector $(\mathrm{Re}(\boldsymbol{g})'\mathrm{Im}(\boldsymbol{g})')'$. Here, because it can be verified that $\mathrm{vec}(H)$ constructed from the "one-ring" model is special complex Gaussian, the second-order statistics of $\mathrm{vec}(H)$ are completely specified by $\mathrm{cov}(\mathrm{vec}(H))$ [19]. The covariance between $H_{l,p}$ and $H_{m,q}$ is

$$\boldsymbol{E}\left[H_{l,p}H^*_{m,q}\right]$$
$$= \frac{1}{2\pi} \int_0^{2\pi} \exp\left\{-\frac{2\pi j}{\lambda}\left[D_{\mathrm{TA}_p \to S(\theta)} - D_{\mathrm{TA}_q \to S(\theta)}\right.\right.$$
$$\left.\left. + D_{S(\theta) \to \mathrm{RA}_l} - D_{S(\theta) \to \mathrm{RA}_m}\right]\right\} d\theta. \quad (5)$$

In general, (5) needs to be evaluated numerically. Fortunately, when Δ is small, which is often the case in fixed wireless applications, an approximation exists that offers useful insights. The approximation is derived using the notation illustrated in Fig. 2. In a two-dimensional plane, let the x-axis be parallel to the line that connects the BS and the SU. Let $d^T(p, q)$ denote the displacement between TA_p and TA_q, and $d^T_x(p, q)$ and $d^T_y(p, q)$ denote the projections of $d^T(p, q)$ on the x- and y-axis, respectively. Similar notations, $d^R(l, m)$, $d^R_x(l, m)$, and $d^R_y(l, m)$,

apply to the SU side. Let Ω_θ denote the angle at which $S(\theta)$ is situated, as viewed from the center of the BS antenna relative to the x-axis. When Δ is small $D_{\mathrm{TA}_p \to S(\theta)} - D_{\mathrm{TA}_q \to S(\theta)} \approx d^T_x(p, q)\cos\Omega_\theta + d^T_y(p, q)\sin\Omega_\theta, \sin\Omega_\theta \approx (R/D)\sin\theta \approx \Delta\sin\theta$, and $\cos\Omega_\theta \approx 1 - (1/2)(R/D)^2\sin^2\theta = 1 - (1/4)(R/D)^2 + (1/4)(R/D)^2\cos 2\theta$. Substituting these approximations into (5)

$$\boldsymbol{E}\left[H_{l,p}H^*_{m,q}\right]$$
$$= \frac{1}{2\pi} \int_0^{2\pi} \exp\left\{-j\frac{2\pi}{\lambda}\left[D_{\mathrm{TA}_p \to S(\theta)}\right.\right.$$
$$\left.\left. - D_{\mathrm{TA}_q \to S(\theta)} + D_{S(\theta) \to \mathrm{RA}_l} - D_{S(\theta) \to \mathrm{RA}_m}\right]\right\} d\theta$$
$$\approx \frac{1}{2\pi} \int_0^{2\pi} \exp\left\{-j\frac{2\pi}{\lambda}\left[d^T_x(p, q)\right.\right.$$
$$\cdot \left(1 - \frac{\Delta^2}{4} + \frac{\Delta^2\cos 2\theta}{4}\right) + \Delta\, d^T_y(p, q)\sin\theta$$
$$\left.\left. + d^R_x(l, m)\sin\theta + d^R_y(l, m)\cos\theta\right]\right\} d\theta. \quad (6)$$

We evaluate (6) for the following special cases (note that $1/(2\pi)\int_0^{2\pi}\exp(jx\cos\theta)\,d\theta = J_0(x)$, where $J_0(x)$ is the Bessel function of the first kind of the zeroth order):

• from one BS antenna element to two SU antenna elements, as

$$\frac{d^R(l, m)}{R} \to 0, \boldsymbol{E}[H_{l,p}H^*_{m,p}] \to J_0\left(\frac{2\pi}{\lambda}d^R(l, m)\right)$$

• from two BS antenna elements aligned on the y-axis to one SU antenna element

$$d^T_x(p, q) = 0, \; \boldsymbol{E}[H_{m,p}H^*_{m,q}] \approx J_0\left(\Delta\frac{2\pi}{\lambda}d^T_y(p, q)\right)$$

• from two BS antenna elements aligned on the x-axis to one SU antenna element

$$d^T_y(p, q) = 0, \; \boldsymbol{E}[H_{m,p}H^*_{m,q}]$$
$$\approx e^{-j(2\pi/\lambda)\,d^T_x(p,q)(1-(1/4)\Delta^2)}J_0$$
$$\cdot \left(\left(\frac{\Delta}{2}\right)^2 \frac{2\pi}{\lambda}d^T_x(p, q)\right).$$

A well-known result for diversity reception systems derived in [12] states that when maximal-ratio combining is employed the degradation in capacity is small even with fading correlation coefficients as high as 0.5. Here, to attain a correlation coefficient

lower than 0.5, the minimum antenna element separations employed by the three cases are 0.24λ, $0.24\Delta^{-1}\lambda$, and $0.96\Delta^{-2}\lambda$, respectively.

If the minimum SU antenna spacing is sufficiently greater than half wavelength, the correlation introduced by finite SU antenna element spacing is low enough that the fades associated with two different SU antenna elements can be considered independent. Mathematically, if the SU antenna spacing is large enough, we will see that the n rows of H can be approximated as i.i.d. complex Gaussian row vectors with covariance matrix Ψ, where $\Psi_{p,q} = \boldsymbol{E}[H_{m,p}H_{m,q}^*]$. Assuming that the rows of H are i.i.d. complex Gaussian vectors with covariance Ψ, the channel covariance matrix is[2] $\mathrm{cov}(\mathrm{vec}(H)) = \Psi \otimes I_{n_R}$. Similarly, if the SU and BS switch their roles as the transmitter and the receiver, under this approximation $\mathrm{cov}(\mathrm{vec}(H)) = I_{n_R} \otimes \Psi$. Note that if $\mathrm{cov}(\mathrm{vec}(H)) = \Psi^R \otimes \Psi^T$, the statistical properties of H are identical to those of the product matrix $AH_wB^\dagger$ where the $n_R \times n_T$ matrix H_w contains i.i.d. $\tilde{N}(0, 1)$ entries, $AA^\dagger = \Psi^T$, and $(BB^\dagger)' = \Psi^R$. In summary, if the fades experienced by different SU antenna elements can be considered independent, the following approximations can be used to analyze the MEA capacity:

$$H \sim H_wB^\dagger \text{ in the downlink (BS to SU) and}$$
$$H \sim AH_w \text{ in the uplink (SU to BS).} \qquad (7)$$

In (7), the notation $x \sim y$ means that "the distribution of x is identical to the distribution of y." In Section IV, we use Monte Carlo simulations to verify that (7) is a good approximation in the sense that the distribution of the eigenvalues of $HH^\dagger$ is closely approximated.

III. ANALYSIS OF MEA CAPACITY

A. Capacity

In the introduction, we mentioned that communication is carried out using bursts (packets). The burst duration is assumed to be short enough that the channel can be regarded as essentially fixed during a burst, but long enough that the standard information-theoretic assumption of infinitely long code block lengths is a useful idealization. These assumptions are expected to be met in, for instance, many fixed wireless and indoor wireless applications. In this quasi-static scenario, it is meaningful to associate a channel capacity with a given realization of channel matrix H. Because the channel capacity is a function of the channel matrix, the channel capacity is a random quantity whose distribution is determined by the distribution of H. An important measure for the channel capacity of an MEA operating in a quasi-static fading environment is the channel capacity at a given outage probability q, denoted by C_q. To be precise, the channel capacity is less than C_q with probability q.

The channel capacity of a communication system described by (2) given the channel realization H under an average transmitter power constraint is [19], [20]

$$C = \max_{tr(\Sigma_s) \leq \rho} \log_2[\det(I + H\Sigma_s H^\dagger)] \text{ (bits/channel use)} \qquad (8)$$

where Σ_s is the covariance matrix of $\boldsymbol{s}$ and ρ is the maximum normalized transmit power. The MEA is an n_T-input n_R-output linear system with i.i.d. AWGN. With linear operations at both the transmitter and the receiver, the MEA can be transformed into an equivalent system consisting of $n = \min(n_T, n_R)$ decoupled single-input single-output (SISO) subchannels. To show this, let the singular value decomposition of the channel matrix H be $H = U_H D_H V_H^\dagger$. The transmitter left-multiplies the signal to be conveyed $\boldsymbol{x}_\tau$ by the unitary matrix V_H. Similarly, the receiver left-multiplies the received signal by $\boldsymbol{r}_\tau$ by $U_H^\dagger$. That is, $\boldsymbol{s}_\tau = V_H \boldsymbol{x}_\tau$, $\boldsymbol{y}_\tau = U_H^\dagger \boldsymbol{v}_\tau$, and $\boldsymbol{u}_\tau = U_H^\dagger \boldsymbol{v}_\tau$. Substituting these into (2), the input–output relationship between $\boldsymbol{x}_\tau$ and $\boldsymbol{y}_\tau$ is

$$\boldsymbol{y}_\tau = D_H \boldsymbol{x}_\tau + \boldsymbol{u}_\tau \qquad (9)$$

where the components of the noise vector $\boldsymbol{u}_\tau$ are i.i.d. $\tilde{N}(0, 1)$. Denote the diagonal entries of the nonnegative diagonal matrix D_H by $\varepsilon_k, k = 1, 2, \cdots, n$. Writing (9) component-wise, we get

$$y_\tau^k = \varepsilon_k x_\tau^k + u_\tau^k. \qquad (10)$$

Therefore, the multiplication of unitary matrices V_H and $U_H^\dagger$ transforms an (n_T, n_R) MEA into n SISO subchannels with (power) gains ε_k^2. Note that ε_k^2 are the eigenvalues of $HH^\dagger$ because $HH^\dagger U_H = U_H D_H^2$. The MEA capacity is the sum of the capacities of the n subchannels [19]. Suppose that a transmit power ρ_k is allocated to the kth subchannel, the MEA capacity is

$$C = \sum_{k=1}^{n} \log_2\left(1 + \rho_k \varepsilon_k^2\right). \qquad (11)$$

The overall transmit power constraint requires that $\sum_{k=1}^{n} \rho_k \leq \rho$. The strategy for distributing the power affects the MEA capacity in (11). Given ε_k^2, the power allocation that maximizes the MEA capacity is calculated through the "water-pouring" algorithm [20]. In many applications, however, it is more practical to allocate equal power to these subchannels [21], i.e., $\rho_k = \rho/n$. The channel capacity with a uniform power allocation constraint is

$$C = \log_2\left(\det\left(I + \frac{\rho}{n}HH^\dagger\right)\right) = \sum_{k=1}^{n} \log_2\left(1 + \frac{\rho}{n}\varepsilon_k^2\right). \qquad (12)$$

Note that if the uniform power distribution is employed, the MEA capacity is independent of V_H. This property makes uniform power allocation a good choice for systems in which the transmitter cannot acquire the knowledge of H. Henceforth, in this paper, we will assume that uniform power allocation is employed.

---

[2]The Kronecker product of matrices M and N is defined as

$$M \otimes N = \begin{bmatrix} M(1, 1)N & M(1, 2)N & \cdots \\ M(2, 1)N & M(2, 2)N & \cdots \\ \cdots & \cdots & \cdots \end{bmatrix}.$$

B. Bounds on MEA Capacity

The distribution of MEA capacity can be calculated given the distribution of ε_k^2. However, for a general spatial fading covariance and a finite spatial dimensionality, the distribution of ε_k^2 can be very difficult to compute. The exact distributions of ε_k^2 and MEA capacity will be studied using Monte Carlo simulations in the next section. Here, we formulate lower and upper bounds on MEA capacity based on the fading statistics (7). To derive these bounds, we need the following mathematical tools.

a) Let H_w be an $n_R \times n_T$ matrix whose entries are i.i.d. $\tilde{N}(0, 1)$. The subscript w is used to mean "white." Denote the QR decomposition of H_w by $H_w = QR$, where Q is an unitary matrix and R is an upper triangular matrix. The upper diagonal entries of R are statistically independent of each other. The magnitude squares of the diagonal entries of R, say $|R_{l,l}|^2$, are chi-squared distributed with $2(n_R - l + 1)$ degrees of freedom. The off-diagonal entries of R are i.i.d. $\tilde{N}(0, 1)$. These can be proved by applying the standard Householder transformation to the matrix H_w [22], [23]. Clearly, $H_w Q_1 \sim Q_2 H_w \sim H_w$ for any unitary matrices Q_1 and Q_2.

b) For any diagonal matrix D and any upper-triangular matrix R

$$\det(DD^\dagger + RR^\dagger) \geq \prod_l \left(|D_{l,l}|^2 + |R_{l,l}|^2 \right).$$

c) For any nonnegative definite matrix A, $\det(A) \leq \prod_l A_{l,l}$.

d) For any unitary matrix Q and any square matrices X and Y, $\det(I + XY) = \det(I + YX)$ and $\det(I + QXQ^\dagger) = \det(I + X)$.

Next, we examine the following two special cases. In the following, we assume that $n_T \leq n_R$.

Case I: The fades are i.i.d. Substituting $H_w = QR$ into (12), the MEA capacity can be lower and upper bounded by, respectively

$$
\begin{aligned}
C &= \log_2\left(\det\left(I + \frac{\rho}{n_T} HH^\dagger \right) \right) \\
&\stackrel{(d)}{=} \log_2\left(\det\left(I + \frac{\rho}{n_T} RR^\dagger \right) \right) \\
&\stackrel{(b)}{\geq} \sum_{l=1}^{n_T} \log_2\left(1 + \frac{\rho}{n_T} |R_{l,l}|^2 \right)
\end{aligned}
\tag{13}
$$

and

$$
\begin{aligned}
C &= \log_2\left(\det\left(I + \frac{\rho}{n_T} RR^\dagger \right) \right) \\
&\stackrel{(c)}{\leq} \sum_{l=1}^{n_T} \log_2\left(1 + \frac{\rho}{n_T}\left(|R_{l,l}|^2 + \sum_{m=l+1}^{n_T} |R_{l,m}|^2 \right) \right).
\end{aligned}
\tag{14}
$$

From a), $|R_{l,l}|^2$ is chi-squared distributed with $2(n_R - l + 1)$ degrees of freedom. Also because $\sum_{m=l+1}^{n_T} |R_{l,m}|^2$ is chi-squared distributed with $2(n_T - l)$ degrees of freedom, $|R_{l,l}|^2 + \sum_{m=l+1}^{n} |R_{l,m}|^2$ is chi-squared distributed with $2(n_R + n_T - 2l + 1)$ degrees of freedom. In short, the MEA capacity is lower-bounded by the sum of the capacities of n_T subchannels whose power gains are independently chi-squared distributed with degrees of freedom $2n_R, 2n_R - 2, \cdots, 2(n_R - n_T + 1)$, and is upper bounded by the sum of the capacities of n_T subchannels whose power gains are independently chi-squared distributed with degrees of freedom $2(n_R + n_T - 1), 2(n_R + n_T - 3), \cdots, 2(n_R - n_T + 1)$. The difference between the mean values of the upper and the lower bounds is no greater than 1 b/s/Hz per spatial dimension. The lower bound was first derived by Foschini in [21]. In fact, Foschini has proved that the mean values of the exact MEA capacity and its lower bound, both normalized to perspatial dimension quantities, converge to the same limit when $n \to \infty$ [21].

Case II: $\mathrm{cov}(\mathrm{vec}(H)) = \Psi \otimes I_{n_R}$ or $I_{n_R} \otimes \Psi$. We have shown in Section II that in the "one-ring" model, if the antenna array inside the scatterer ring (usually the SU) employs a sufficiently large antenna element spacing, the fading covariance matrix can be approximated by $\Psi \otimes I_{n_R}$ in the downlink (BS to SU) and $I_{n_R} \otimes \Psi$ in the uplink (SU to BS), and the approximations in (7) apply. Note that if $\mathrm{cov}(\mathrm{vec}(H)) = \Psi \otimes I_{n_R}$ for some nonnegative definite Ψ, the distributions of ε_k^2 and hence the distribution of MEA capacity can be exactly calculated using the techniques developed for Wishart matrices [22]. However, the calculation is generally very difficult because it involves the zonal polynomials, which are notoriously difficult to compute. Furthermore, the actual computation does not give us as much insight into the problem.

Substituting H by $AH_w B^\dagger$ into (12), we have

$$
\begin{aligned}
C &\sim \log_2\left[\det\left(I + \frac{\rho}{n_T} AH_w B^\dagger (AH_w B^\dagger)^\dagger \right) \right] \\
&\stackrel{(a)(d)}{\sim} \log_2\left[\det\left(I + \frac{\rho}{n_T} H_w D_B^2 H_w^\dagger D_A^2 \right) \right].
\end{aligned}
\tag{15}
$$

Here D_A and D_B are diagonal matrices whose diagonal elements are the singular values of A and $B^\dagger$, respectively. The diagonal entries of both D_A and D_B are ordered in descending order of their magnitudes down the diagonal. Substituting $H_w = QR$ and $A = I$ in (15), the capacity in the downlink can be bounded by

$$
\begin{aligned}
C &\sim \log_2\left[\det\left(I + \frac{\rho}{n_T} H_w D_B^2 H_w^\dagger \right) \right] \\
&\stackrel{(b)(d)}{\geq} \sum_{l=1}^{n_T} \log_2\left(1 + \left(\frac{\rho}{n_T}\right) |D_{B(l,l)}|^2 |R_{l,l}|^2 \right)
\end{aligned}
\tag{16}
$$

and

$$
\begin{aligned}
C &\stackrel{(c)(d)}{\leq} \sum_{l=1}^{n_T} \log_2\left(1 + \left(\frac{\rho}{n_T}\right) |D_{B(l,l)}|^2 \right. \\
&\qquad \left. \cdot \left(|R_{l,l}|^2 + \sum_{m=l+1}^{n_T} |R_{l,m}|^2 \right) \right).
\end{aligned}
\tag{17}
$$

Similar to the case when the fades are i.i.d., the MEA capacity is still lower and upper bounded by the total capacity of n independent SISO subchannels, and the difference between the mean values of the upper and the lower bound is less than 1 b/s/Hz per spatial dimension. Due to the spatial fading correlation, the power gain of the lth subchannel is scaled

by a factor of $|D_{B(l,l)}|^2$ (or, on decibel scale, augmented by $10 \log_{10} |D_{B(l,l)}|^2$ dB). Note that because the trace of D_B^2 is equal to n_T, when compared to the situation in which the fades are i.i.d., the path gains of some subchannels are scaled up while others are scaled down.

When the number of antenna elements is large, determining the MEA capacity through simulation is very computation-intensive. The upper bound in (17) can be employed to investigate the capacity when the number of antenna elements is large. Let $\boldsymbol{E}(C)$ denote the mean value of MEA capacity at a fixed average total power constraint ρ. For any concave function $f(x)$, $\boldsymbol{E}(f(x)) \leq f(\boldsymbol{E}(x))$. Thus, an upper bound of $\boldsymbol{E}(C)$, denoted by $\overline{\boldsymbol{E}}(C)$, in the downlink direction can be derived from (17) by substituting the mean values of chi-squared random variables for them

$$
\begin{aligned}
\boldsymbol{E}(C) &\leq \sum_{l=1}^{n_T} \log_2 \Bigg(1 + \frac{\rho}{n_T} |D_{B(l,l)}|^2 \boldsymbol{E} \\
&\quad \cdot \left(|R_{l,l}|^2 + \sum_{m=l+1}^{n} |R_{l,m}|^2 \right) \Bigg) \\
&= \sum_{l=1}^{n_T} \log_2 \left(1 + \frac{\rho}{n_T} |D_{B(l,l)}|^2 (n_R + n_T - 2l + 1) \right) \\
&\equiv \overline{\boldsymbol{E}}(C).
\end{aligned}
\tag{18}
$$

Note that due to the normalization used in this paper, the mean value of a chi-squared random variable with $2k$ degrees of freedom is k.

For example, we employ (18) to investigate the effect of angle spread on the relation between $\overline{\boldsymbol{E}}(C)$ and the number of antenna elements $n = n_R = n_T$. The result is displayed in Fig. 3. (The definitions of broadside and inline linear antenna arrays will be given in Section IV.)

C. Effective Degrees of Freedom

We have shown in (11) that an (n_T, n_R) MEA can be decomposed into an equivalent system of $n = \min(n_T, n_R)$ SISO subchannels whose path power gains are the eigenvalues of $HH^\dagger$. Based on this decomposition, one would intuitively expect that the capacity of an (n, n) MEA system should grow roughly linearly with n for a given fixed transmitted power, because if $(\rho \varepsilon_k^2 / n) \gg 1$ for $k = 1, 2, \cdots, n$, (12) can be approximated by

$$
C(\rho) \approx \sum_{k=1}^{n} \log_2 \left(\frac{\rho \varepsilon_k^2}{n} \right).
\tag{19}
$$

However, this high SNR condition may not be met in practice. For an (n, n) MEA, if $(\rho \varepsilon_k^2) / n$ is much smaller than one for some k, the capacity provided by the kth subchannel is nearly zero. This may occur when the communication system operates in a low SNR setting, e.g., in long-range communication application or transmission from low-power devices. On the other hand, it may occur if with significant probability ε_k^2 is very small, which is a direct result of severe fading correlation. Here we introduce the concept of effective degrees of freedom

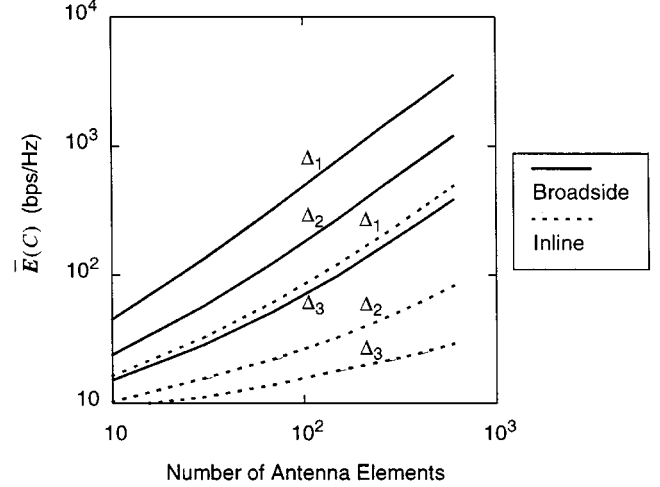Fig. 3. The effect of angle spread Δ on the relationship between the upper bound of mean capacity $\overline{\boldsymbol{E}}(C)$ and the number of antenna elements $n = n_R = n_T$. The fixed overall power constraint is $\rho = 18$ dB.

(EDOF), which is a parameter that represents the number of subchannels actively participating in conveying information under a given set of operating conditions. It is well known that for an SISO channel, at high SNR, a G-fold increase in the transmitter power results in an increase in the channel capacity of $\log_2 G$ b/s/Hz. If a system is equivalent to EDOF SISO channels in parallel, the capacity of the system should increase by (EDOF $\cdot \log_2 G$) b/s/Hz when the transmitter power is raised by a factor of G. In light of this, we define EDOF at a given transmit power ρ and outage probability q to be

$$
\text{EDOF} \equiv \left. \frac{d}{d\delta} C_q(2^\delta \rho) \right|_{\delta=0}.
\tag{20}
$$

We note that EDOF is a real number in $[0, n]$. Although the $n_R \times n_T$ channel matrix H has rank n with probability one in general, the power allocated to $(n - \text{EDOF})$ out of the n dimensions is very poorly utilized. EDOF is determined by the fading correlation. It is also affected by SNR; the value of EDOF is higher when SNR is increased.

For an example of how fading correlation affects EDOF, consider the fading correlation in the "one-ring" model when the angle spread approaches zero. In such a case, $|E[h_{l,p} h_{l,q}^*]| \to 1$. Therefore, the n columns of H are perfectly correlated, and only one of the n eigenvalues of $HH^\dagger$ has significant probability of being practically nonzero. The overall effect is that as the angle spread approaches zero, EDOF approaches one. An (n, n) MEA thus degenerates to a $(1, n)$ MEA.

IV. SIMULATION RESULTS

In this section, we present the capacity of multielement antenna systems obtained from Monte Carlo simulations. Simulation is necessary because computing the distributions of MEA capacity, subchannel gains, and subchannel capacities analytically is very difficult. The results in this section illustrate the effect of the antenna geometry and the physical dimensions of the scattering environment on the statistics of MEA capacity. Another goal is to verify that (7) is a good approximation to the exact channel distribution.
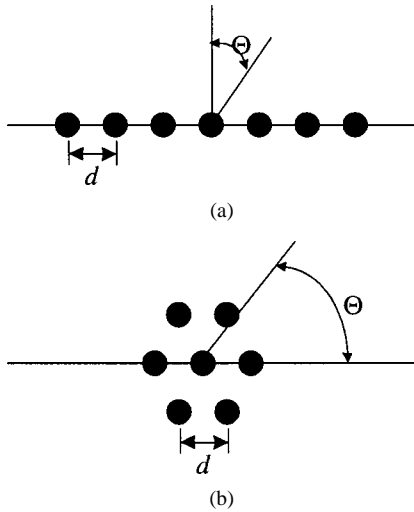
Fig. 4. Antenna set arrangement. Note the definitions of the angle of arrival Θ and the minimum antenna element spacing d. (a) Linear-array MEA and (b) hexagon MEA.

A. Simulation Algorithm

Fig. 4 shows the arrangement of antenna elements. We have chosen a fixed number of antenna elements $n_T = n_R = 7$. In Fig. 4(a), seven antenna elements are equally spaced along an axis. This is referred to as a linear-array MEA. In Fig. 4(a) we also define the angle of arrival Θ at the BS for the linear-array MEA. Following conventional notation [6], we use the term "broadside" and "inline" to refer to the situations when $\Theta = 0°$ and $\Theta = 90°$, respectively. In Fig. 4(b), seven antennas are arranged on a hexagonal planar array. This is referred to as the hexagon MEA. For planar antenna sets, the hexagonal arrangement achieves the highest antenna density per unit area for a given nearest-neighbor antenna spacing. Furthermore, the effects of the angle of arrival are not significant, due to the symmetry of the hexagon. Three configurations are considered: broadside and inline linear-array antenna set at the BS with inline linear-array antenna set at the SU, and hexagon antenna sets at both the BS and the SU. The nearest-neighbor separations between antenna elements of the BS and the SU antenna sets are denoted by dt and dr, respectively. Again, the BS and the SU assume the roles of the transmitter and the receiver, respectively.

Given Δ, dt, and dr, one way to generate the channel realization is to randomly select the angular positions and phases of the equivalent scatterers and compute H using ray tracing. When the number of scatterers is large, an equivalent way is as follows. First, compute the channel covariance matrix $\mathrm{cov}(\mathrm{vec}(H))$ from (6). Let $\Psi = \mathrm{cov}(\mathrm{vec}(H))$ and $\Psi = \Psi^{1/2}(\Psi^{1/2})^{\dagger}$. The instances of H can then be generated by premultiplying a white channel $\mathrm{vec}(H_w)$ by $\Psi^{1/2}$. That is

$$\mathrm{vec}(H) = \Psi^{1/2}\mathrm{vec}(H_w). \tag{21}$$

We generated 10 000 instances of channel and collected the statistics of MEA capacity and ordered eigenvalues of $HH^{\dagger}$. The average received SNR ρ is chosen to be 18 dB. For comparison purposes, the 10% outage channel capacities $C_{0.1}$ of $(1, 1)$, $(1, 7)$, and $(7, 7)$ systems over i.i.d. Rayleigh-fading channels given $\rho = 18$ dB are 2.94, 7.99, and 32.0 b/s/Hz, respectively.

B. Simulation Results

The physical parameters in the "one-ring" model include the angle spread, angle of arrival, antenna spacing, and antenna arrangement. First, we investigate the effect of angle spread Δ. Fig. 5(a) shows the complementary cumulative distribution function (c.c.d.f.) of channel capacity of the hexagon MEA versus Δ. The support of the transition region of the c.c.d.f. curve moves toward lower capacity values as the angle spread decreases. Note that when the angle spread is extremely small ($\Delta < 0.6°$), the c.c.d.f. of the $(7, 7)$ MEA is identical to that of a $(1, 7)$ diversity reception system with maximal-ratio combining. Fig. 5(b) shows $C_{0.1}$ for the three configurations of MEA versus Δ. For all three, $C_{0.1}$ decreases monotonically as the angle spread decreases. Intuitively, because the difference in path lengths from two transmitting antenna elements to any scatterer becomes smaller as Δ decreases, it becomes increasingly difficult for the receiver to distinguish between the transmissions of the various transmitting antenna elements. Mathematically, the correlation between the columns of H increases as Δ decreases. Fig. 5(c) shows that the EDOF of each type of MEA indeed decreases as the angle spread decreases.

The simulation also provides the probability density functions (pdf's) of the ordered eigenvalues of $HH^{\dagger}$. The magnitude of ε_k^2 is best displayed in decibel units. Let $\mu_k = 10 \log_{10} \varepsilon_k^2$, and let $p_k(\mu_k)$ denote the pdf of μ_k. Fig. 6 displays $p_k(\mu_k)$. As the angle spread Δ decreases, the following is observed: a) the median of μ_1 increases slightly; b) the medians of μ_k, $k \geq 2$ decrease; and c) the difference between the medians of μ_k and μ_{k+1} increases for all k. These observations indicate that statistically, as Δ decreases, the disparity among μ_k, i.e., the disparity among the subchannels in (10), increases. The pdf's ε_k^2 also provide a convenient way to estimate the EDOF. The average received SNR necessary to obtain a certain EDOF can be estimated from Fig. 6 as follows. For a natural number z, the average received SNR necessary for EDOF $= z$ is approximately α, where α is determined by $\int_{\alpha}^{\infty} p_z(\mu_z)\, d\mu_z = 0.9$.

Second, we investigate the effect of the BS antenna spacing dt. Fig. 7(a) shows the c.c.d.f. of channel capacity of the hexagon MEA in the large angle spread setting ($D = 1000\lambda$, $\Delta = 15°$, $dr = 0.5\lambda$). We find that the channel capacity increases greatly as dt increases. In Fig. 7(a), similar to Fig. 5(a), the support of the transition part of the c.c.d.f. curve moves toward higher capacity values as dt increases. Fig. 7(b) and (c) displays the relation between $C_{0.1}$ and dt for the three types of MEA in the large and small ($D = 100\,000\lambda$, $\Delta = 0.6°$, $dr = 0.5\lambda$) angle spread settings, respectively. Given a fixed dt, the capacity of a $(7, 7)$ broadside linear-array MEA is always higher than that of a $(7, 7)$ hexagon MEA, which in turn is always higher than that of a $(7, 7)$ inline linear-array MEA. In Section II, we showed that the effectiveness of reducing the fading correlation by increasing the BS antenna spacing along the axes perpendicular and parallel to the direction of wave arrival are different. To attain zero fading correlation with inline linear-array MEA's, the BS antenna spacing must be $4/\Delta$ times of the spacing required when using
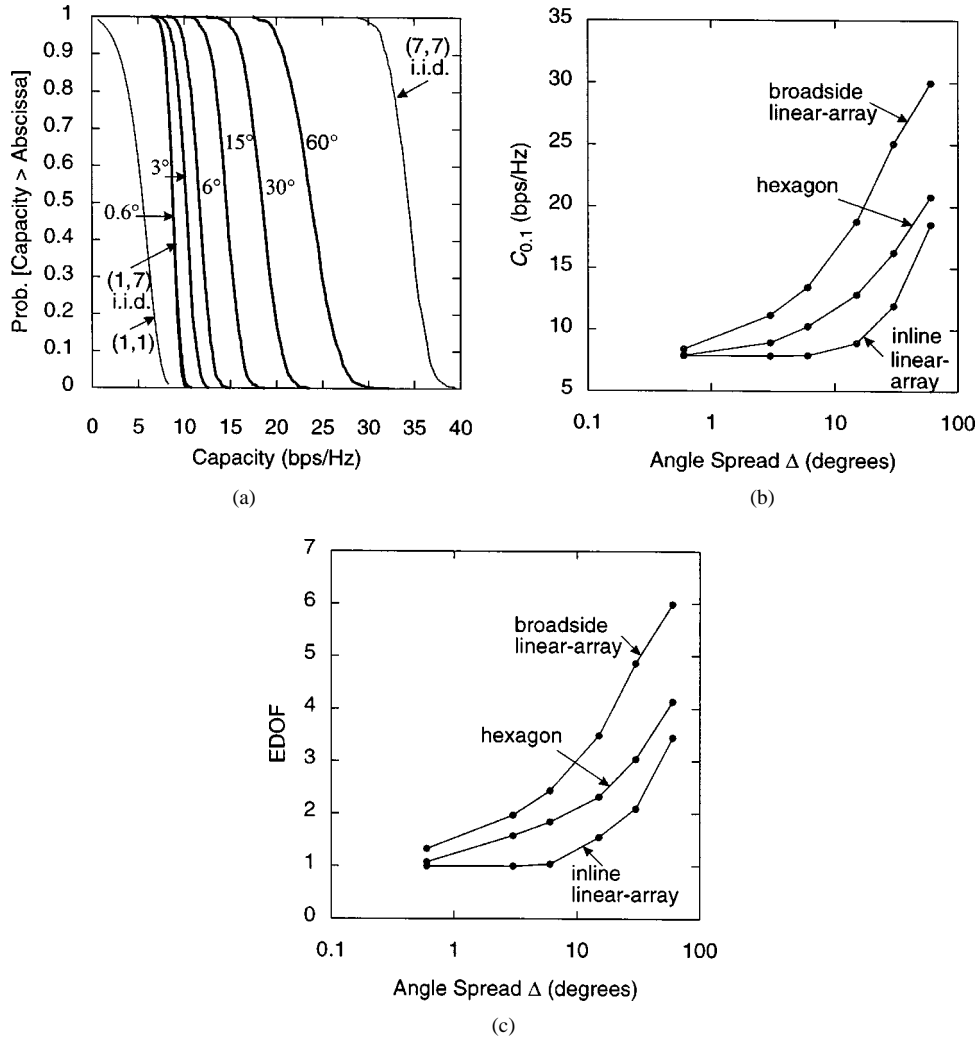
(a)

(b)

(c)

Fig. 5   (a) The c.c.d.f. of channel capacity for hexagon MEA given various angle spreads. $dt = dr = 0.5\lambda$. The reference curves are the c.c.d.f.'s of channel capacity when assuming H is a 7×7, 1×7, and 1×1 matrix with i.i.d. $\bar{N}(0, 1)$ entries, respectively. (b) $C_{0.1}$ versus angle spread. (c) EDOF versus angle spread.
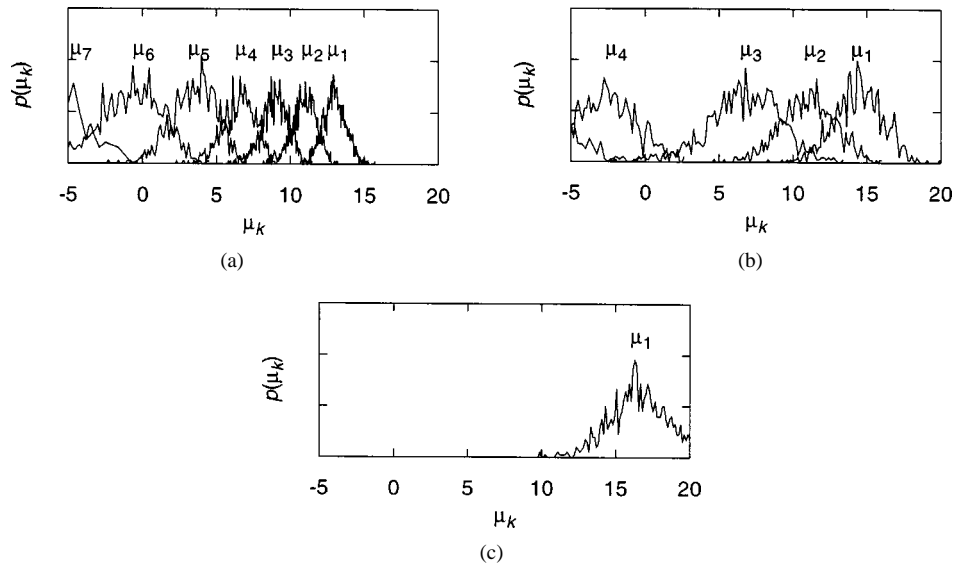

(a)

(b)

(c)

Fig. 6.   The pdf's of the ordered eigenvalues of $HH^{\dagger}$ based on the "one-ring" model. Here, ε_k^2 is the kth largest eigenvalue of $HH^{\dagger}$ and $p(\mu_k)$ is the pdf of $\mu_k = 10 \log_{10} \varepsilon_k^2$. The pdf's are normalized to have the same height for display purpose: (a) $(7, 7)$ MEA with i.i.d. fades; (b) $(7, 7)$ hexagon MEA with a large angle spread ($\Delta = 60°$); and (c) $(7, 7)$ hexagon MEA with a small angle spread ($\Delta = 0.6°$).
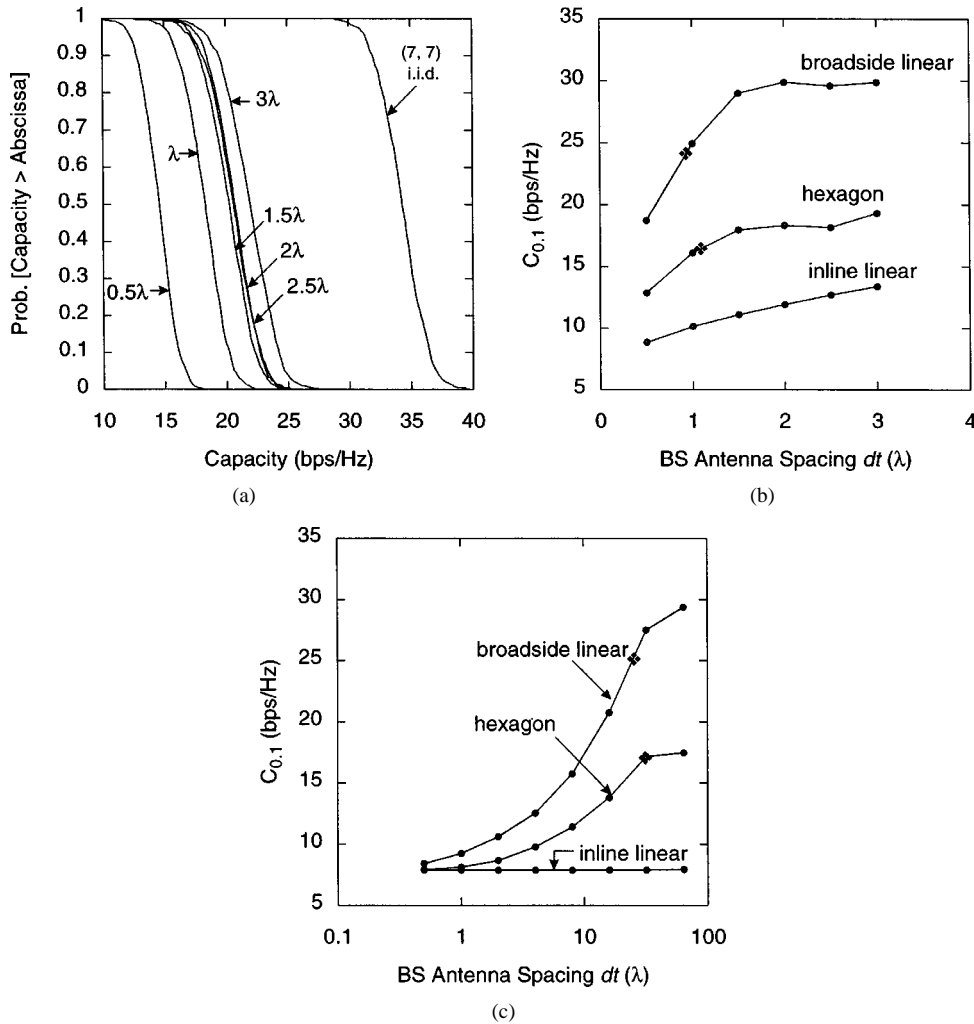
Fig. 7. (a) The c.c.d.f. of capacity of (7, 7) hexagon MEA with $\Delta = 15°$, $dr = 0.5\lambda$. (b) $C_{0.1}$ versus dt for large angle spread ($\Delta = 15°$, $dr = 0.5\lambda$). (c) $C_{0.1}$ versus dt for small angle spread ($\Delta = 0.6°$, $dr = 0.5\lambda$). In (b) and (c), we use ♦ to mark the smallest dt with which the maximum fading correlation coefficient is 0.5. After the maximum fading correlation coefficient is reduced to under 0.5, the benefit of increasing dt starts to saturate.

broadside linear-array MEA's. The difference in effectiveness is confirmed here by simulation. Note that because the Bessel function governing the relation between antenna spacing and fading correlation is not monotonic, the MEA capacity does not decrease monotonically as dt is decreased. This can be seen in Fig. 7(b).

Third, we examine the effect of the SU antenna spacing dr. Fig. 8(a) shows the c.c.d.f. of channel capacity of the hexagon MEA in the large angle spread setting ($D = 1000\lambda$, $\Delta = 15°$, $dt = 0.5\lambda$). Fig. 8(b) and (c) displays $C_{0.1}$ versus dr in the large and small ($D = 100\,000\lambda$, $\Delta = 0.6°$, $dr = 0.5\lambda$) angle spread settings, respectively. The c.c.d.f. curves of MEA capacity become steeper as dr increases. This results in an improvement in $C_{0.1}$, but such an improvement is not nearly as significant as the capacity improvement while increasing dt. The analysis in Section II explains the striking difference between increasing the antenna spacing at the BS and at the SU, in terms of effectiveness in improving MEA capacity. Once the antenna spacing at the SU is more than a half wavelength, the correlation coefficient between any two entries on a column of H is generally lower than 0.5. The fading correlation is already low and therefore cannot be reduced significantly by increasing dr.

We conclude that the angle spread and the BS antenna spacing perpendicular to the direction of wave arrival at the BS dominates the channel correlation and thus the channel capacity. If the direction of wave arrival is known to a reasonable accuracy, it is advantageous to deploy a broadside linear-array MEA. On the other hand, if omnidirectional coverage is the goal, an MEA with a symmetric shape, such as the hexagon MEA, is clearly the better choice.

Fig. 9 compares the eigenvalue distributions of $HH^\dagger$ and $(H_wB^\dagger)(H_wB^\dagger)^\dagger$ given the parameters $dt = dr = 3\lambda$ and $\Delta = 15°$ and $0.6°$. Very good agreement is observed. The results in Fig. 8 also show that the overestimate of channel capacity caused by assuming the rows of H are uncorrelated is not substantial. These results demonstrate that (7) is a valid approximation in the downlink if the SU employs an antenna spacing sufficiently large.

V. SUMMARY

In previous studies that analyzed MEA capacity, a common assumption is that the fades between pairs of transmit–receive antenna elements are independent. However, in real propagation
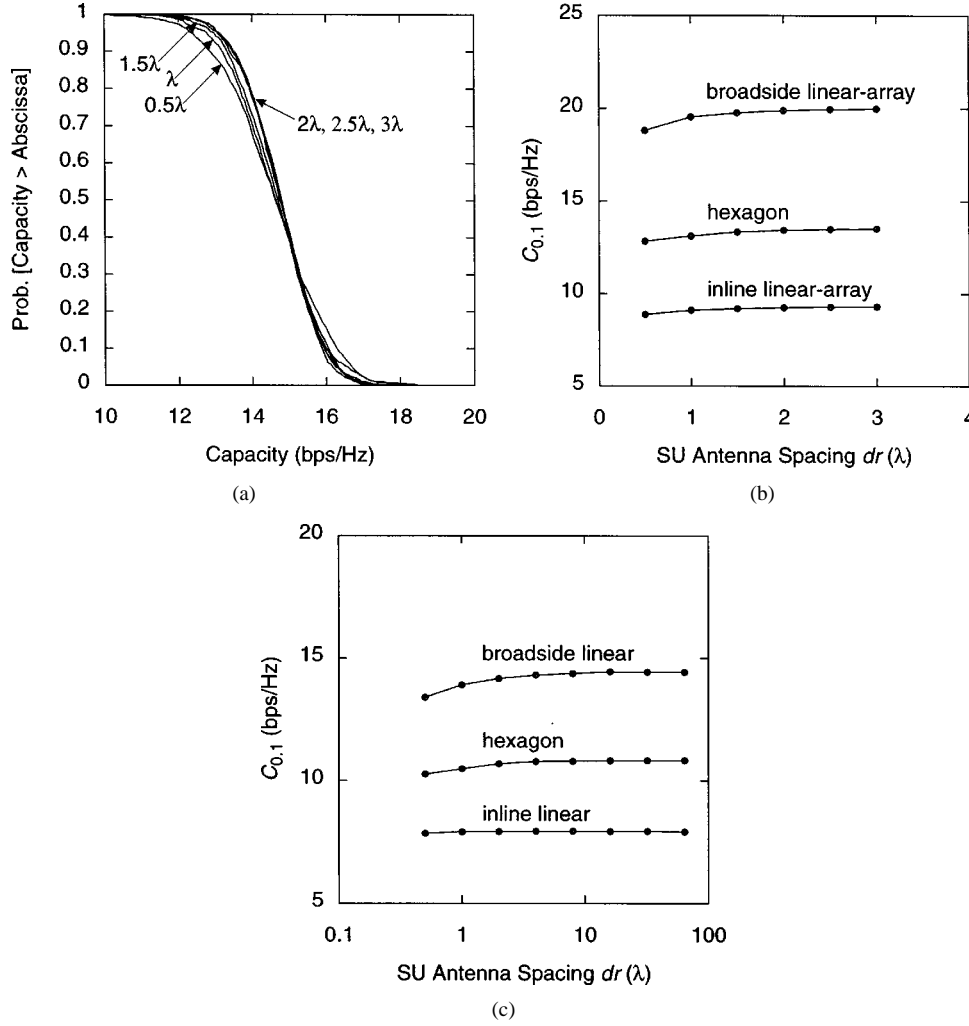
(a)

(b)

(c)

Fig. 8. (a) The c.c.d.f. of capacity of $(7, 7)$ hexagon MEA at various values of dr with $\Delta = 15°$, $dt = 0.5\lambda$. (b) $C_{0.1}$ versus dr for large angle spread $(\Delta = 15°$, $dt = 0.5\lambda)$. (c) $C_{0.1}$ versus dr for small angle spread $(\Delta = 0.6°$, $dt = 5\lambda)$.
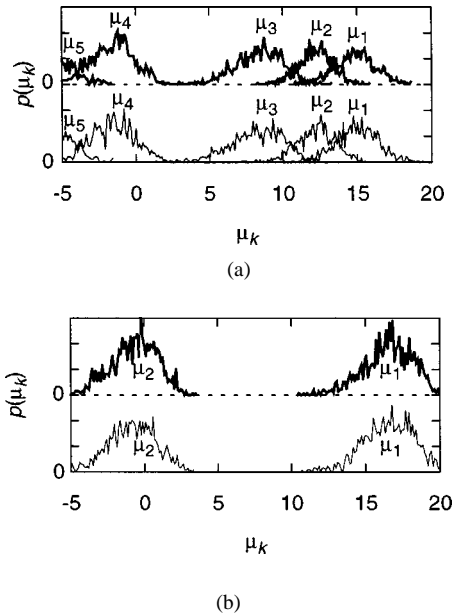

(a)

(b)

Fig. 9. The distributions of the eigenvalues of $HH^\dagger$ (thick, elevated curves) and $H_w B^\dagger (H_w B^\dagger)^\dagger$ (thin curves) given the parameters $dt = dr = 3\lambda$ and $\Delta = 15°$ (a) and $0.6°$ (b).

environment, fading correlation does exist and can potentially lead to a capacity lower than that predicted with the i.i.d. fading assumption. In this paper, we started by modeling the multipath propagation environment with an abstract model. From the model, we determine the spatial fading correlation and its effect on the MEA capacity.

The "one-ring" model can reasonably represent a scattering environment in which one of the communicating parties, the SU, is surrounded by local scatterers. The channel correlation based on the "one-ring" model is a function of antenna spacing, antenna arrangement, angle spread, and the angle of arrival. When the angle spread is small, expressions for approximate fading correlation can be formulated to highlight the differences between how the SU antenna element spacing and the BS antenna element spacing (both parallel to and perpendicular to the direction of wave arrival) contribute to the fading correlation.

We showed that an (n_T, n_R) MEA consists of $n = \min(n_T, n_R)$ SISO subchannels, or eigenmodes. The MEA capacity is the sum of the individual subchannel capacities. The gains of these subchannels are the n largest eigenvalues of $HH^\dagger$. The distribution of these gains is determined by the fading correlation.

To investigate the effect of fading correlation on MEA capacity analytically, we considered the situations in which the antenna element spacing at the SU is sufficient that the correlation among the entries on any column of the channel matrix is negligible. We showed that the capacity of an (n, n) MEA can be lower (upper) bounded by the sum of the capacities of n decoupled subchannels with independent path power gains that are scaled chi-squared distributed random variables with $2, 4, \cdots, 2n\,(2, 6, \cdots, 4n-2)$ degrees of freedom. The scaling factors depend on the fading correlation. The stronger the fading correlation, the higher the disparity between the capacities of these subchannels. As the fading correlation becomes more severe, more and more subchannels have gains too small to convey information at any significant rate. We defined the parameter EDOF to represent the number of subchannels that actively contribute to the overall MEA capacity.

We performed Monte Carlo simulations to study quantities that are very difficult to compute analytically, such as the distributions of the eigenvalues of $HH^\dagger$ and the MEA capacity. The results confirm our analysis. The angle spread is a key parameter; the MEA capacity generally decreases as the angle spread decreases. The BS antenna separation perpendicular to the direction of wave arrival is also a very important factor. If the direction of wave arrival is known approximately, it is advantageous to deploy a broadside linear-array MEA with a large antenna spacing; but if omnidirectional coverage is the goal, an MEA with a symmetric shape, such as the hexagon MEA, is clearly the best choice.

ACKNOWLEDGMENT

REFERENCES

[1] G. J. Foschini and M. J. Gans, "On limits of wireless communication in a fading environment when using multiple antennas," *Wireless Personal Commun.*, vol. 6, no. 3, pp. 311–335, Mar. 1998.

[2] G. J. Foschini and R. A. Valenzuela, "Initial estimation of communication efficiency of indoor wireless channel," *Wireless Networks*, vol. 3, pp. 141–154, 1997.

[3] J. H. Winters, J. Salz, and R. D. Gitlin, "The impact of antenna diversity on the capacity of wireless communication systems," *IEEE Trans. Commun.*, vol. 42, pp. 1740–1751, Feb. 1994.

[4] J. H. Winters, "On the capacity of radio communication systems with diversity in a Rayleigh fading environment," *IEEE J. Select. Areas Commun.*, vol. SAC-5, pp. 871–878, June 1987.

[5] C. Chuah, J. M. Kahn, and D. Tse, "Capacity of multi-antenna array systems in indoor wireless environment," in *Globecom 98*, Sydney, 1998.

[6] W. C. Y. Lee, "Effects on correlation between two mobile radio base-station antennas," *IEEE Trans. Commun.*, vol. COM-21, pp. 1214–1224, Nov. 1973.

[7] W. C. Y. Lee, "Antenna spacing requirement for a mobile radio base-station diversity," *Bell Syst. Tech. J.*, vol. 50, pp. 1859–1874, 1971.

[8] S. P. Stapleton, T. McKeen, and X. Carbo, "Mobile communications base station array antenna: Characterization of the environment," in *Proc. IEEE 46th Vehicular Technology Conf.*, vol. 3, Atlanta, GA, May 1996, pp. 1858–1862.

[9] S. B. Rhee and G. I. Zysman, "Results of suburban base-station spatial diversity measurements on the UHF band," *IEEE Trans. Commun.*, vol. COM-22, pp. 1630–1634, Oct. 1974.

[10] R. B. Ertel, P. Cardieri, K. W. Sowerby, T. S. Rappaport, and J. H. Reed, "Overview of spatial channel models for antenna array communication systems," *IEEE Pers. Commun.*, vol. 5, pp. 10–22, Feb. 1998.

[11] W. C. Jakes, *Microwave Mobile Communications*. New York: Wiley, 1974, pp. 60–65.

[12] J. Salz and J. H. Winters, "Effect of fading correlation on adaptive arrays in digital wireless communications," in *Proc. IEEE Vehicular Technology Conf.*, vol. 3, 1993, pp. 1758–1774.

[13] J. Fuhl, A. F. Molisch, and E. Bonek, "Unified channel model for mobile radio systems with smart antennas," *Proc. Inst. Elect. Eng. Radar, Sonar Navig.*, vol. 145, no. 1, pp. 32–41, Feb. 1998.

[14] G. G. Raleigh and J. M. Cioffi, "Spatio-temporal coding for wireless communications," *IEEE Trans. Commun.*, vol. 46, pp. 357–366, Mar. 1998.

[15] P. F. Driessen and G. J. Foschini, "Deploying multiple transmit antennas to greatly enhance capacity in wireless channels," *IEEE Trans. Commun.*, vol. 47, pp. 173–176, Feb. 1999.

[16] J. Litva and T. K. Lo, *Digital Beamforming in Wireless Communications*. Boston, MA: Artech, 1996.

[17] J. M. Wozencraft and I. M. Jacobs, *Principles of Communication Engineering*. New York: Wiley, 1965, pp. 527–532.

[18] G. J. Foschini and J. Salz, "Digital communications over fading radio channels," *Bell Syst. Tech. J.*, vol. 62, pp. 429–456, Feb. 1983.

[19] E. I. Telatar and D. Tse, "Capacity and mutual information of broad-band multipath fading channels," in *Proc. IEEE Int. Symp. Information Theory*, 1998, p. 188.

[20] T. M. Cover and J. A. Thomas, *Elements of Information Theory*. New York: Wiley, 1991.

[21] G. J. Foschini, "Layered space-time architecture for wireless communication in a fading environment when using multi-element antennas," *Bell Labs Tech. J.*, Autumn 1996.

[22] R. J. Muirhead, *Aspects of Multivariate Statistical Theory*. New York: Wiley, 1982.

[23] M. S. Barlett, "On the theory of statistical regression," in *Proc. R. Soc. Edinb.*, vol. 53, 1933, pp. 260–283.

Da-Shan Shiu (M'99–S'95) received the B.S.E.E. degree from National Taiwan University, Taipei, Taiwan, in 1993, and the Ph.D. degree in electrical engineering and computer sciences from the University of California at Berkeley in 1999. His current research interests include wireless optical communications, space–time signal processing, smart antenna, and spread-spectrum communications.

He is currently with Qualcomm Incorporated, Santa Clara, CA. His current research interests include wireless optical communications, space-time signal processing, smart antenna, and spread spectrum communications.

Dr. Shiu is a member of Phi Tau Phi.

Gerard J. Foschini (F'86) received the B.S.E.E. degree from the New Jersey Institute of Technology, Newark, NJ, in 1961, the M.E.E. degree from New York University, New York, NY, in 1963, and the Ph.D. degree in mathematics from Stevens Institute of Technology, Hoboken, NJ, in 1967.

In 1961, he joined Bell Laboratories. He has been involved with data communications research on many kinds of systems. He has done research on point-to-point systems as well as on networks. Recently, he has worked on multiple antenna wireless communications and on wave-division multiplexed optical communications systems. He is temporarily on leave from wireless communication research to work in the area of optical communication theory, where he is concentrating on analyzing both polarization mode dispersion and the information theory implications of fiber nonlinearities. He has also taught at Princeton University, Princeton, NJ, and Rutgers University, New Brunswick, NJ.

Michael J. Gans received the Ph.D. degree in electrical engineering from the University of California at Berkeley, in 1965.

In 1966, he joined Bell Laboratories, where he is currently on staff at the Wireless Communications Research Department in Holmdel, NJ. He received the Ph.D. degree in electrical engineering from the University of California at Berkeley, in 1965. His primary research interests include mobile radio, antennas, satellites, fiber optics, and infrared communications.

Joseph M. Kahn (M'87–SM'98) received the A.B., M.A., and Ph.D. degrees in physics from the University of California at Berkeley, in 1981, 1983, and 1986, respectively. His doctoral research involved infrared spectroscopy of hydrogen-related impurity complexes in semiconductors.

He is a Professor and Vice Chairman in the Department of Electrical Engineering and Computer Sciences at the University of California at Berkeley. From 1987 to 1990, he was a Member of the Technical Staff in the Lightwave Communications Research Department of AT&T Bell Laboratories, where he performed research on multigigabit-per-second coherent optical fiber transmission systems and related device and subsystem technologies. He joined the faculty of U. C. Berkeley in 1990. His current research addresses several areas of communications, including infrared and radio wireless communications, source and channel coding techniques, and optical fiber communications.

Dr. Kahn received the National Science Foundation Presidential Young Investigator Award in 1991. He is a member of the IEEE Communications Society and the IEEE Lasers and Electro-Optics Society. He is serving currently as a Technical Editor of *IEEE Personal Communications Magazine*.